Dynamo action in the transition to buoyancy-dominated anelastic convection

Radostin D. Simitev[a,b,c], Friedrich H. Busse[b,d], Alexander G. Kosovichev[a]

[a] *W.W. Hansen Experimental Physics Laboratory, Stanford University – Stanford CA 94305, USA*
[b] *Department of Earth and Space Sciences, University of California, Los Angeles – Los Angeles, CA 90095, USA*
[c] *School of Mathematics and Statistics, University of Glasgow – Glasgow G12 8QW, UK, EU*
[d] *Institute of Physics, University of Bayreuth – Bayreuth 95440, Germany*

Abstract

Keywords: Convection, Differential rotation, Solar convection zone

---

1. Summary

- Non-magnetic convection in the buoyancy dominated-regime has been studied but DYNAMO SOLUTIONS HAVE NOT.
- In the Buoyancy-dominated regime differential rotation naturally decreases towards the surface. This may produce dynamo waves propagating TOWARD THE EQUATOR.
- Are the convective columns still HIDING beneath the cellular convection.

Email address: `Radostin.Simitev@glasgow.ac.uk` (Radostin D. Simitev)

2. Introduction

2.1. Motivation

- Dynamo action in the transition from rotation-dominated regime to buoyancy-dominated regime has not been previously studied. This transition has been investigated but only in non-magnetic convection by Arnou et al using the Boussinesq approximation and by Gastine et all (2012) using the anelastic approximation. The rotation-dominated is characterised with prograde differential rotation, while the buoyancy-dominated regime is characterised with retrograde differential rotation due to vigorous mixing of angular momentum.

- The results may be relevant to Neptune and Uranus. There is evidence that the magnetic field of Uranus is non-dipolar (provide references) and that the differential rotation is retrograde at the equator. Retrograde differential rotation naturally develops in the buoyancy-dominated regime and it is of interest whether the magnetic fields that are generated resemble that of Neptune and Uranus.

- The results may be relevant as a model of Solar magnetic field oscillations, structure of the Solar convection zone, and differential rotation.

  - **Solar cycle –** The direction of dynamo waves in self-consistent simulations with prograde differential rotation is always from equator to poles in contrast to observations. We wish to check whether retrograde differential rotation generated in the buoyancy-dominated regime may reverse the direction of dynamo waves so that they propagate from poles to equator in agreement with observations.
  - **Structure of convection zone –** It will be of interest to find whether different regimes of convection may develop in the inner and at the outer part of the shell simultaneously so that organised geostrophic convection is hidden below a near-surface layer of well-mixed ("turbulent") convection. We believe that such a configuration is similar to the structure of the Solar convection zone. Indeed, it is well established by observation of the surface velocities and magnetic fields that buoyancy effects dominate near the surface. As a result the near-surface flows and magnetic fields are strongly turbulent and lack any global organization. On the other hand, the regularity of the 11-year Solar cycle is also well established and the regular reversals cannot be achieved without large-scale organized field and flow. We would like to argue that the organized columnar structures that are characteristic in the rotation-dominated regime will play this role.

    Variation in density is a necessary ingredient in this scenario. Indeed, in the Boussinesq approximation, the rotation parameter τ and the critical Rayleigh number R_c are constant throughout the shell. This means that the entire volume of the shell will be either in the rotation-dominated or the buoyancy-dominated regime. In contrast, the anelastic approximation allows for radial variation in density, viscosity and entropy diffusivity so that τ and R_c vary with radius. In this way, one may hope to achieve a configuration where the inner part of the shell is in the rotation-dominated regime and the outer part is in the buoyancy-dominated regime.

– **Solar differential rotation –** Finally, differential rotation may also assume more Solar-like profile.

- In fact, variation in density only may not be sufficient to produce Solar-like differential rotation as indicated by Gastine et al. In this case convection flows in the rotation-dominated region are relatively weaker by comparison with flows in the buoyancy-dominated near-surface layer. A stronger organized flow is likely needed to produce the solar-lice cyclic oscillations and differential rotation profile.

3. Mathematical model and numerical method

3.1. Anelastic equations

We consider an electrically conducting perfect gas confined to a spherical shell. The shell rotates with a fixed angular velocity $\Omega\hat{\boldsymbol{k}}$ about the vertical axis and an entropy contrast ΔS is imposed between its inner and outer surfaces. Assuming a gravity field proportional to $1/r^2$, we find a hydrostatic polytropic reference state of the form

$$\overline{\rho} = \rho_c \zeta^n, \quad \overline{T} = T_c \zeta, \quad \overline{P} = P_c \zeta^{n+1}, \quad \zeta = c_0 + c_1 d/r, \tag{1}$$

with parameters $c_0 = (2\zeta_o - \eta - 1)/(1-\eta)$, $c_1 = (1+\eta)(1-\zeta_o)/(1-\eta)^2$, $\zeta_o = (\eta+1)/(\eta \exp(N_\rho/n) + 1)$. The parameters ρ_c, P_c and T_c are reference values of density, pressure and temperature at the middle of the shell, and n, N_ρ and η are defined further below. Convection and magnetic field generation set in for sufficiently large values of the entropy contrast, ΔS, and can be described by the equations of continuity, momentum, energy and magnetic flux. In the annelastic approximation (Gough, 1969; Jones et al., 2011) these equations take the form

$$\nabla \cdot \overline{\rho}\boldsymbol{u} = 0, \quad \nabla \cdot \boldsymbol{B} = 0, \tag{2a}$$

$$\partial_t \boldsymbol{u} + (\nabla \times \boldsymbol{u}) \times \boldsymbol{u} = -\nabla\Pi - \tau(\hat{\boldsymbol{k}} \times \boldsymbol{u}) + \frac{\mathrm{R}}{\mathrm{Pr}}\frac{S}{r^2}\hat{\boldsymbol{r}} + \boldsymbol{F}_\nu + \frac{1}{\overline{\rho}}(\nabla \times \boldsymbol{B}) \times \boldsymbol{B}, \tag{2b}$$

$$\partial_t S + \boldsymbol{u} \cdot \nabla S = \frac{1}{\mathrm{Pr}\overline{\rho}\overline{T}}\nabla \cdot \overline{\kappa\rho}\overline{T}\nabla S + \frac{c_1 \mathrm{Pr}}{\mathrm{R}\overline{T}}\left(Q_\nu + \frac{1}{\mathrm{Pm}\overline{\rho}}Q_j\right) \tag{2c}$$

$$\partial_t \boldsymbol{B} = \nabla \times (\boldsymbol{u} \times \boldsymbol{B}) + \mathrm{Pm}^{-1}\nabla^2 \boldsymbol{B}, \tag{2d}$$

where $\boldsymbol{u}$ is the velocity, $\boldsymbol{B}$ is the magnetic flux density, S is the entropy and $\nabla\Pi$ includes all terms that can be written as gradients. The viscous force, and the viscous and Joule heating,

$$\boldsymbol{F}_\nu = \zeta^{-n}\nabla \cdot \boldsymbol{S}, \quad Q_\nu = \boldsymbol{S} : \boldsymbol{e}, \quad Q_j = (\nabla \times \boldsymbol{B})^2, \tag{3}$$

are defined in terms of the deviatoric stress tensor

$$S_{ij} = 2\overline{\nu\rho}(e_{ij} - e_{kk}\delta_{ij}/3), \quad e_{ij} = (\partial_i u_j + \partial_j u_i)/2,$$

where double-dots (:) denotes the Frobenius inner product. We assume that the viscosity and the entropy diffusivity vary in radius as $\overline{\nu}(r) = \nu_c \overline{\rho}^k$ and $\overline{\kappa}(r) = \kappa_c \overline{\rho}^k$ with some negative power $k < 0$, where ν_c and κ_c are their reference values at midshell. We nondimensionalise the governing equations using the thickness of the shell $d = r_o - r_i$ as a unit of length, d^2/ν_c as a unit of time, ΔS as a unit of entropy, $\nu_c\sqrt{\mu_0\rho_c}/d$ as a unit of magnetic induction, ρ_c as a unit of density and T_c as a unit of temperature. Here, r_i and r_o are the inner and the outer radius, λ and μ_0 are the magnetic diffusivity and permiability, respectively. The system is then characterized by eight dimensionless parameters: the radius ratio, the polytropic index, the density scale number, the radial dependence power, the Rayleigh number, the ordinary and the magnetic Prandtl numbers and the Coriolis number, defined as

$$\eta = r_i/r_o, \quad n, \quad N_\rho = \ln\left(\overline{\rho}(r_i)/\overline{\rho}(r_o)\right), \quad k,$$
$$\mathrm{R} = \frac{c_1 T_c d^2 \Delta S}{\nu_c \kappa_c}, \quad \mathrm{Pr} = \frac{\nu_c}{\kappa_c}, \quad \mathrm{Pm} = \frac{\nu_c}{\lambda}, \quad \tau = \frac{2\Omega d^2}{\nu_c}, \tag{4}$$

respectively.

Since the mass flux $\overline{\rho}\boldsymbol{u}$, and the magnetic flux density $\boldsymbol{B}$ are solenoidal vector fields, it is advantageous to employ a decomposition in poloidal and toroidal components,

$$\overline{\rho}\boldsymbol{u} = \nabla \times (\nabla \times \hat{\boldsymbol{r}} r v) + \nabla \times \hat{\boldsymbol{r}} r^2 w, \tag{5a}$$
$$\boldsymbol{B} = \nabla \times (\nabla \times \hat{\boldsymbol{r}} h) + \nabla \times \hat{\boldsymbol{r}} g. \tag{5b}$$

Equations (2a) are then satisfied by construction. Scalar equations for v and w are obtained, and effective pressure gradients are eliminated by taking $\hat{\boldsymbol{r}} \cdot \nabla \times \nabla\times$ and $\hat{\boldsymbol{r}} \cdot \nabla\times$ of equation (2b). Similarly, equations for h and g are obtained by taking $\hat{\boldsymbol{r}} \cdot \nabla\times$ and $\hat{\boldsymbol{r}}\cdot$ of equation (2d). The resulting poloidal-toroidal equations are somewhat lengthy and will not be listed here (or may be listed in an appendix). A minor disadvantage of this representation is that a fourth-order poloidal equation is obtained.

3.2. *Boundary conditions*

We explore various assumptions for the boundary conditions imposed on velocity, entropy and magnetic flux at the surface of the shell. The alternatives are listed below and the particular choice will be specified in each individual case. On a no-slip, impenetrable boundary we impose

$$v = 0, \quad \partial_r v = 0, \quad w = 0. \tag{6}$$

On a stress-free, impenetrable boundary we require

$$v = 0, \quad \partial_r^2 v - \frac{\overline{\rho}'}{\overline{\rho} r}\partial_r(rv) = 0, \quad \partial_r w - \frac{\overline{\rho}'}{\overline{\rho}} w = 0. \tag{7}$$

Values of the entropy may be fixed at the boundaries, then

$$S = 1 \text{ at } r = r_i, \qquad S = 0 \text{ at } r = r_o. \tag{8}$$

Alternatively, the entropy flux may be specified at the top,

$$\partial_r S = 0 \text{ at } r = r_o. \tag{9}$$

Boundary conditions for the magnetic field may be derived from the assumption of an electrically insulating external region, then the poloidal function h is matched to a function $h^{(e)}$, which describes an external potential field,

$$g = 0, \quad h - h^{(e)} = 0, \quad \partial_r (h - h^{(e)}) = 0. \tag{10}$$

Alternatively, a perfectly conducting external region may be assumed, then

$$\partial_r g = 0, \quad h = 0. \tag{11}$$

The, so-called, "pseudo-vacuum" condition offers a third choice,

$$g = 0, \quad \partial_r h = 0. \tag{12}$$

3.3. Numerical method

For the numerical solution of the problem we have adapted the pseudo-spectral method described by Tilgner (1999). The scalar unknowns v, w, h, g and S, are expanded in Chebychev polynomials T_p in the radial direction r, and in spherical harmonics in the angular directions (θ, φ) e.g.,

$$v = \sum_{l=1}^{N_l} \sum_{m=-l}^{l} \sum_{p=0}^{N_r} V_{lp}^m(t)\, T_p\big(x(r)\big)\, P_l^m(\cos\theta)\, \exp(im\varphi), \tag{13}$$

where P_l^m denotes the associated Legendre functions, $x(r) = 2(r - r_i) - 1$, and N_r and N_r are truncation parameters. A system of equations for the coefficients in these expansions is obtained by a combination of a Galerkin spectral projection of the governing equations in the angular directions and a collocation constraint in radius. Computation of nonlinear terms in spectral space is expensive, so nonlinear products and the Coriolis term are computed in physical space and then projected to spectral space at every time step. A standard 3/2-dealiasing in θ and φ is used at this stage. A hybrid of a Crank-Nicolson scheme for the diffusion terms and a second order Adams-Bashforth scheme for the nonlinear terms is used for integration in time.

A range of numerical resolutions has been used in this study varying from ($N_r = 61$, $N_l = 96$) in less demanding cases to ($N_r = 121$, $N_l = 144$) in more stratified or turbulent runs. Correspondingly, the physical gridpoints on which non-linear terms are evaluated have been varied up to $N_r = 121$, $N_\theta = 216$, $N_\varphi = 437$.

3.4. Diagnostic output quantities

Our numerical convection and dynamo solutions are characterized by their kinetic and magnetic energy and heat transport given by a Nusselt number. The energies can be conveniently split into mean and fluctuating components, into poloidal and toroidal components and further into equatorially-symmetric and -antisymmetric components, thus giving a rather complete description of the scales of the convective flow and the multipole structure of dynamos. The mean and fluctuating toroidal and poloidal components of the kinetic energy are defined as

$$\overline{E}_p = \langle (\nabla \times (\nabla \overline{v} \times \boldsymbol{r}))^2 / (2\overline{\rho}) \rangle, \quad \overline{E}_t = \langle (\nabla r \overline{w} \times \boldsymbol{r})^2 / (2\overline{\rho}) \rangle, \tag{14a}$$

$$\check{E}_p = \langle(\nabla \times (\nabla\check{v} \times \boldsymbol{r}))^2/(2\bar{\rho})\rangle, \quad \check{E}_t = \langle(\nabla r\check{w} \times \boldsymbol{r})^2/(2\bar{\rho})\rangle, \tag{14b}$$

where angular brackets $\langle\rangle$ denote averages over the spherical volume of the shell. Magnetic energy components are defined analogously with h and g replacing v and w and without the factor $\bar{\rho}^{-1}$ within the angular brackets. The total energies are, of course, the sum of all components. The Nusselt number is defined as the ratio between the values of the luminosity of the convective state and of the basic conduction state,

$$Nu = -\frac{\exp(N_\rho) - 1}{4\pi n c_1 \bar{\rho}(r_i)^n} \int_{\partial V} \kappa\bar{\rho}\bar{T}(\partial_r S)\boldsymbol{r}^2 \sin\theta d\theta d\varphi,$$

with the integral taken over the top surface ∂V. Apart from quantifying the heat transport of convection, the value of the Nusselt serves as a convenient proxy for the supercriticallity of the solution.

Other diagnostic quantities that are sometimes used to quantify convective and dynamo solutions can be derived from these quantities. For example, a non-dimensional magnetic Reynolds number, Rossby number and Lorentz number are given by

$$Rm = \mathrm{Pm}\sqrt{2E_{\mathrm{kin}}}, \quad Ro = \frac{2}{\tau}\sqrt{2E_{\mathrm{kin}}}, \quad Lo = \frac{2}{\tau}\sqrt{2E_{\mathrm{mag}}},$$

respectively.

4. Benchmarking and validation

To perform the numerical simulations of this study, we have extended our mature Boussinesq code (Tilgner and Busse, 1997; Simitev and Busse, 2005; Busse and Simitev, 2006, 2008; Simitev and Busse, 2009, 2012) to solve the anelastic problem described in section 3. Despite similarities with the Boussinesq code, this extension has proven to be a major modification both in terms of the mathematical model and the numerical code. In order to validate the new code, here we wish to report a comparison with the anelastic dynamo benchmarks recently proposed by Jones et al. (2011). To aid comparison with the latter paper in this section only we employ the alternative nondimensionalisation used in (Jones et al., 2011) where the magnetic diffusion timescale rather that the viscous diffusion scale is employed. Our output results from the three benchmark cases defined in (Jones et al., 2011) are summarized in table 1, and selected components of the solution are plotted in **??**. We achieve near exact agreement with the results reported in (Jones et al., 2011) for the hydrodynamic case and the steady dynamo case, labeled B1 and B2 in table 1. Our results for the unsteady dynamo case labeled B3 in table 1 show some insignificant differences from the values reported in (Jones et al., 2011). The mean zonal flow we obtain in this case is 33% larger than that reported in the benchmark paper even though the angular momentum of our run remains smaller than 10^{-3}. This somewhat larger differential rotation gives rise to a magnetic field with energy 6% larger than that reported in the benchmark paper. The reasons for the discrepancy are that the length of our run is only 0.3 ohmic diffusion times, and that we have imposed a two-fold azimuthal symmetry in this case to reduce computing time.

5. Transition from rotation-dominated regime to buoyancy-dominated regime

Question: Is the transition abrupt?

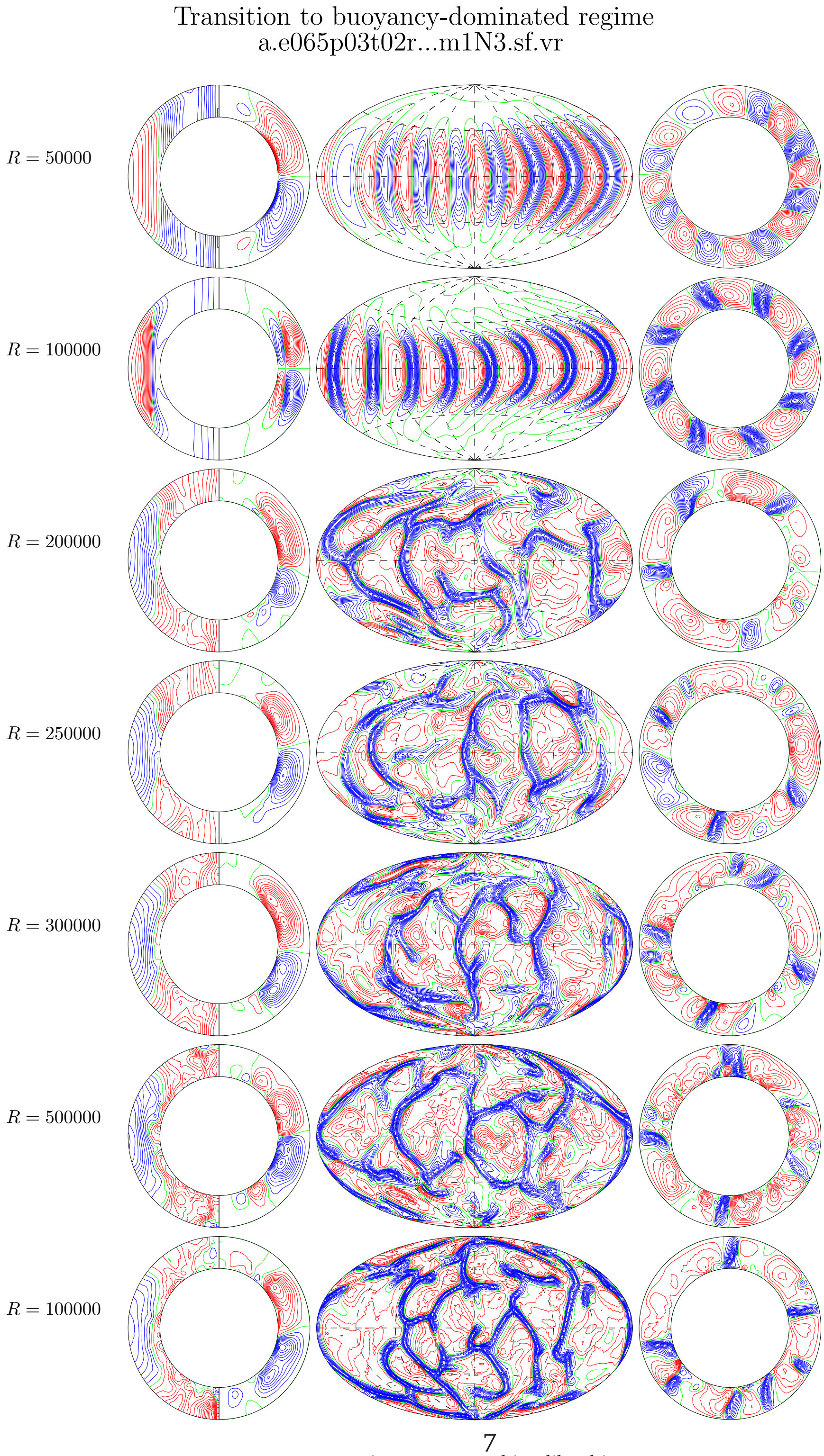

Figure 1: Something like this.

	B1 - Hydrodyn. convection	B2 - Steady dynamo	B3 - Unsteady dynamo
η	0.35	0.35	0.35
n	2	2	2
N_ρ	5	3	3
P	1	1	2
P_m	1	50	2
τ	2000	1000	40000
R	351806	80000	2.5e7
N_r / N_r	129 / 129	129 / 129	111 / 111
N_l / N_θ	128 / 128	128 / 128	120 / 144
N_m / N_φ	129 / 257	129 / 257	121 / 145
Timestep	4e-6	1e-6	1e-7
E	81.87991	4.19405e5	2.32730e5
$\overline{E}_p$	0.02201	53.0100	100.40
$\overline{E}_t$	9.37598	6.01725e4	1.81399e4
M	–	3.20172e5	2.58012e5
$\overline{M}_p$	–	1.69650e4	2.91155e4
$\overline{M}_t$	–	2.41185e5	1.17292e4
Luminosity	4.19886	11.50302	42.50992
Period	to be	inserted	–
Frequency ω	to be	inserted	–
$\boldsymbol{u}_\phi$ at $u_r = 0$	to be	inserted	–
S at $u_r = 0$	to be	inserted	–

Table 1: Comparison with the benchmark solutions proposed in Jones et al. (2011).

Figure 2: Plots of magnetic structures of dynamos as a function of R across the transition.

6. Dynamos in the transition regime

Question: How does the magnetic field shift the transition? - Probably happens at lower R?

7. Evidence of two-layered convection and dynamos

Question: How solar-like are the differential rotation profiles?

Acknowledgements

This research has been supported by NASA Grant NNX-09AJ85G. Computations have been carried out using the NASA Advanced Supercomputing Resources, the US NSF Extreme Science and Engineering Digital Environment (XSEDE). RDS acknowledges a period of study leave granted by the University of Glasgow.

Figure 3: Magnetic and kinetic energies as a function of R across the transition.

Figure 4: Poloidal field lines of best case.

References

Busse, F.H., Simitev, R., 2006. Parameter dependences of convection-driven dynamos in rotating spherical fluid shells. Geophys. Astrophys. Fluid Dyn. 100, 341.

Busse, F.H., Simitev, R., 2008. Toroidal flux oscillations as possible causes of geomagnetic excursions and reversals. Phys. Earth Planet. Inter. 168, 237.

Gough, D.O., 1969. The anelastic approximation for thermal convection. J. Atmos. Sci. 26, 448.

Jones, C.A., Boronski, P., Brun, A.S., Glatzmaier, G.A., Gastine, T., Miesch, M.S., Wicht, J., 2011. Anelastic convection-driven dynamo benchmarks. Icarus 216, 120–135.

Simitev, R., Busse, F.H., 2005. Prandtl-number dependence of convection-driven dynamos in rotating spherical fluid shells. J. Fluid Mech. 532, 365.

Simitev, R., Busse, F.H., 2009. Bistability and hysteresis of dipolar dynamos generated by turbulent convection in rotating spherical shells. EPL 85, 19001.

Simitev, R., Busse, F.H., 2012. How far can minimal models explain the solar cycle? Astrophys. J. 749, 9.

Tilgner, A., 1999. Spectral methods for the simulation of incompressible flows in spherical shells. Int. J. Numer. Meth. Fluids 30, 713–724.

Tilgner, A., Busse, F., 1997. Finite-amplitude convection in rotating spherical fluid shells. J. Fluid Mech. 332, 359–376.

Figure 5: Differenial rotation of best case.